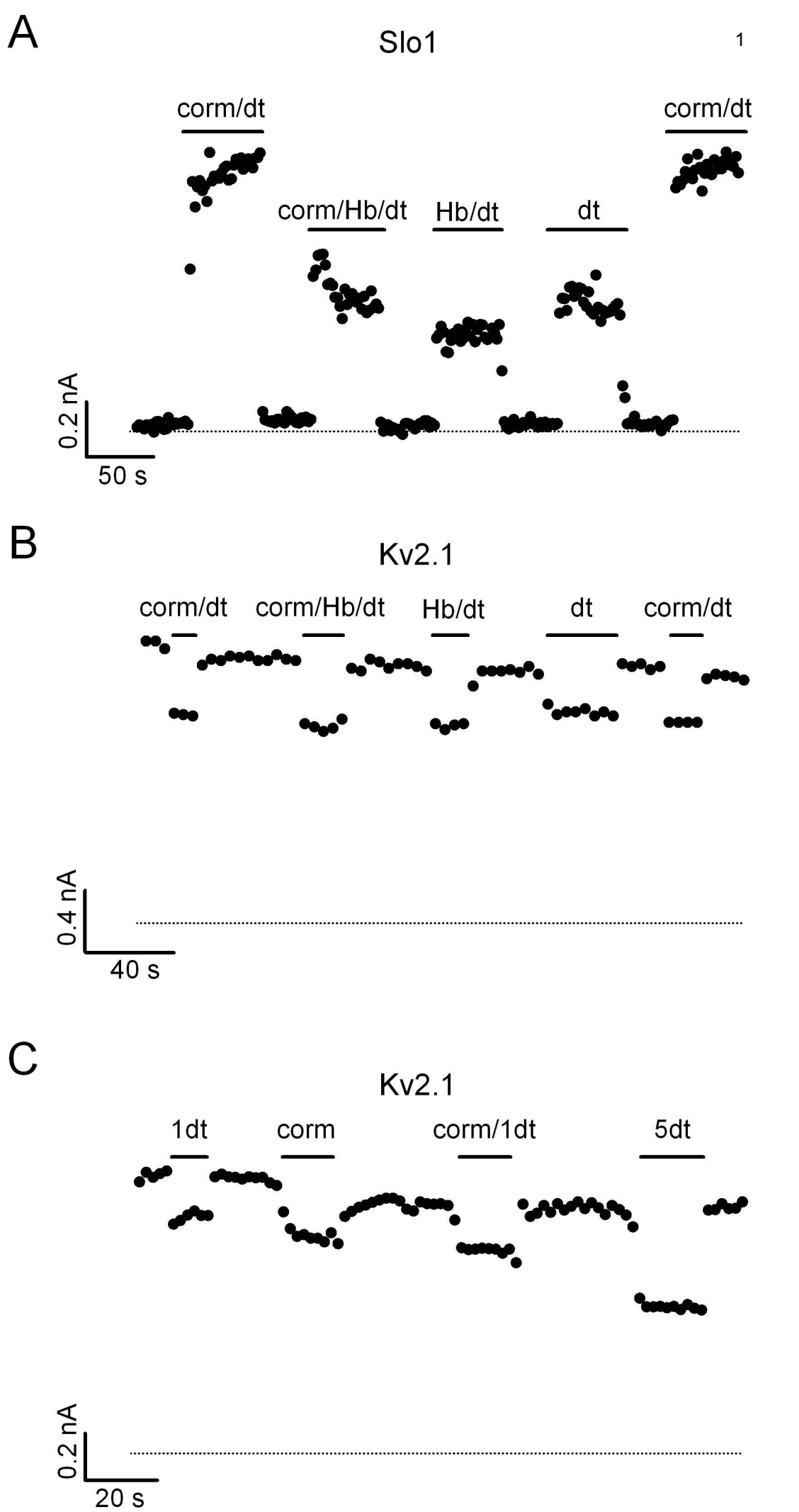

Supplementary Figure 1

A

```
                       M                                           M    V     M    W           V,W                    V,W
Kv2.1       VCIAWFTMEYLLRFLSSPKKWKFFKGPL----RRVVQIFRIMRILRILKLARHSTGLQSLGFTLRRSYNELGLL---ILFLAMGIMIFSSLVFFAEKD---GLCCIAGVLVIALPIP
                      264                                         312  317   323  327         337                    396
Kv1.2       LCIIWFSFEFLVRFFACPSKAGFFTNIM----LAILRVIRLVRVFRIFKLSRHSKGLQILGQTLKASMRELGLL---IFFLFIGVILFSSAVYFAEAD---SLCAIAGVLTIALPVP
                      261   S3                         S4         313  318   324  328         338 S5                 397  S6
```

B

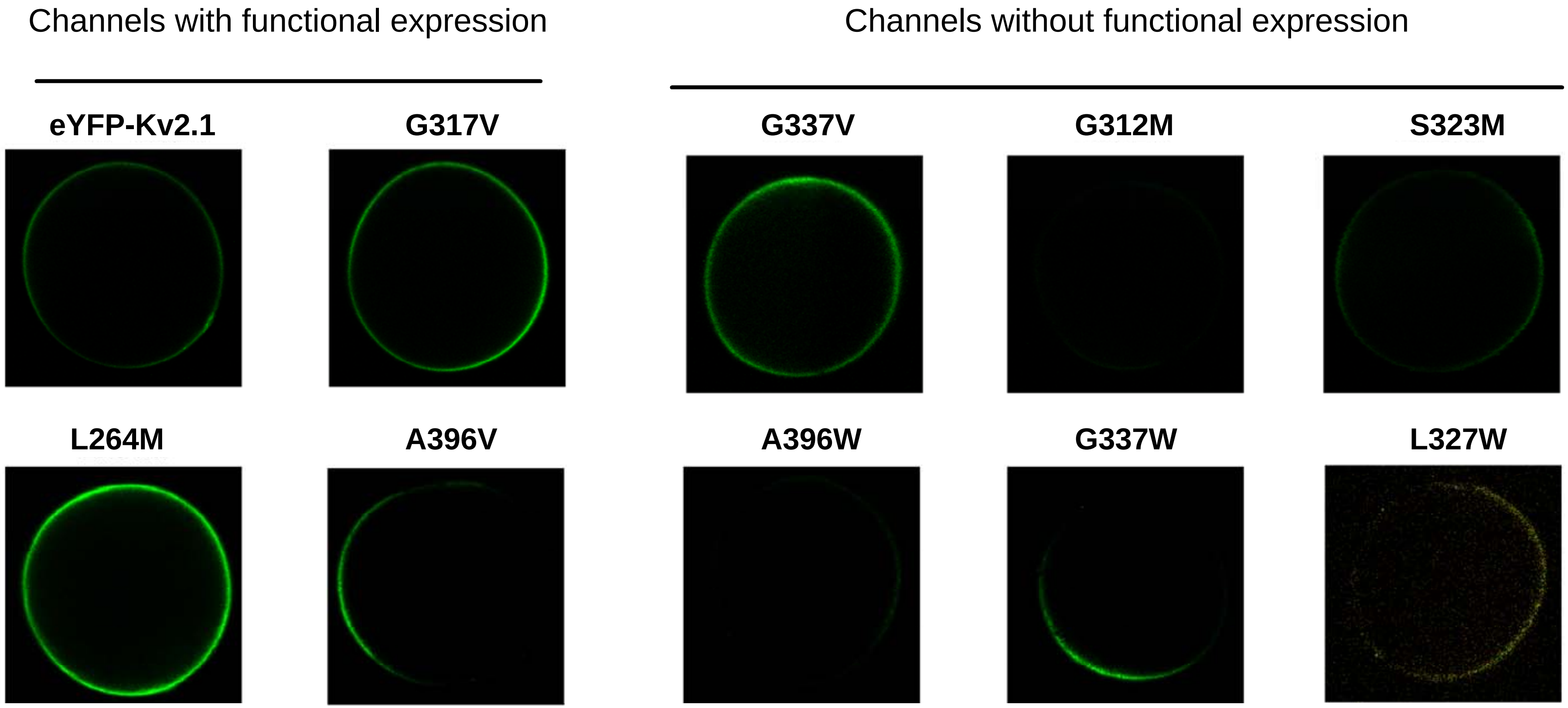

Supplementary Fig. 2

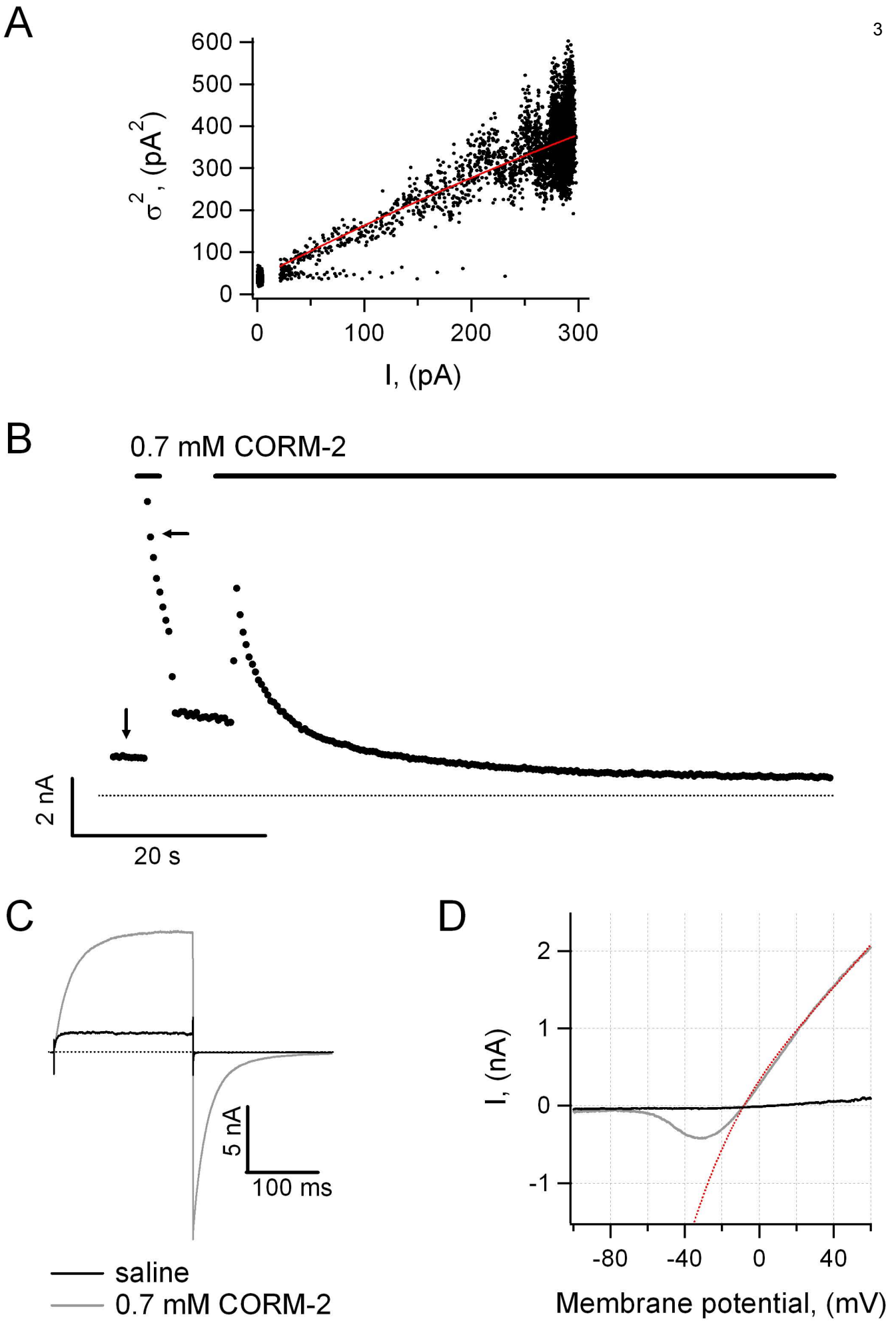

Supplementary Figure 3

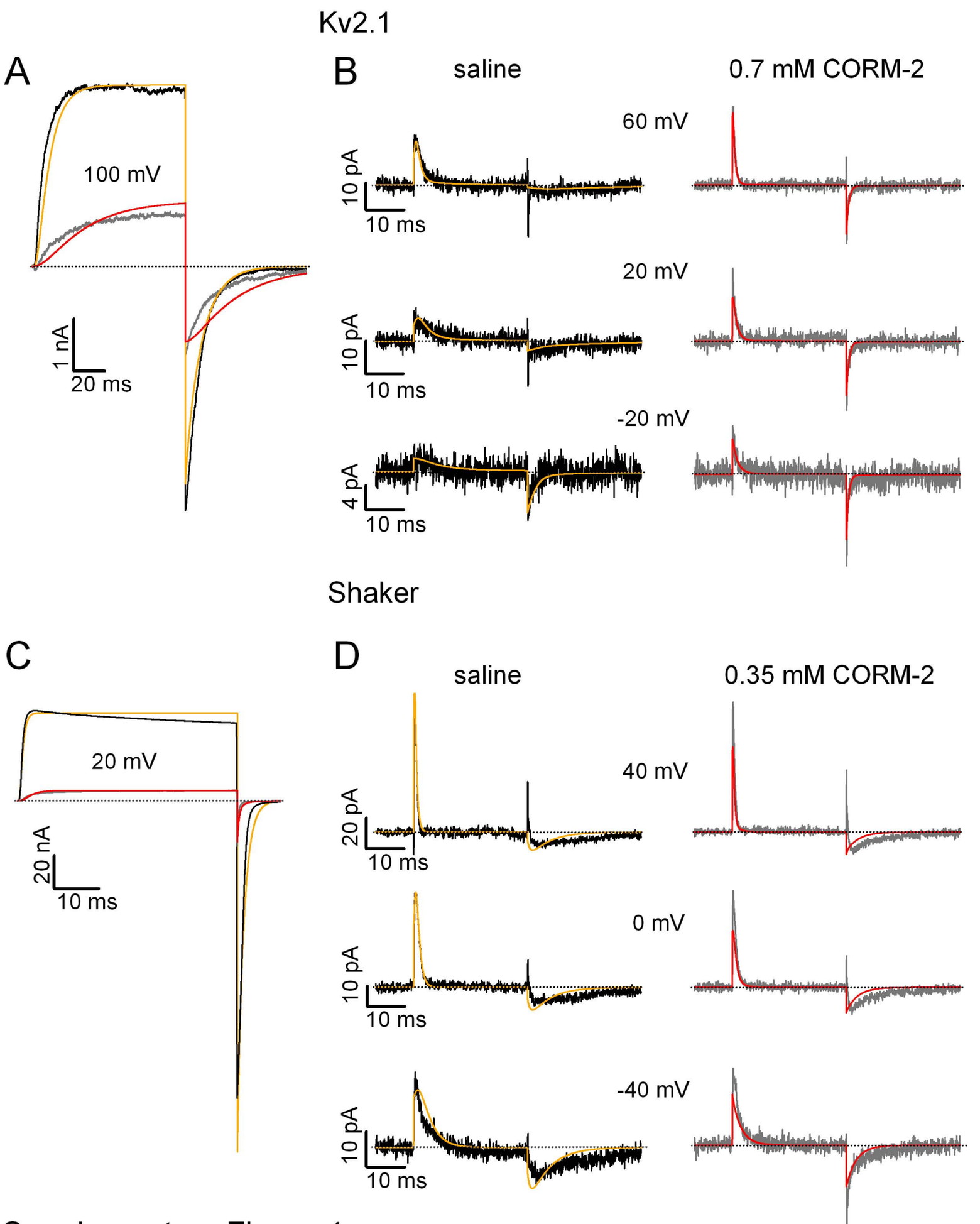

Supplementary Figure 4

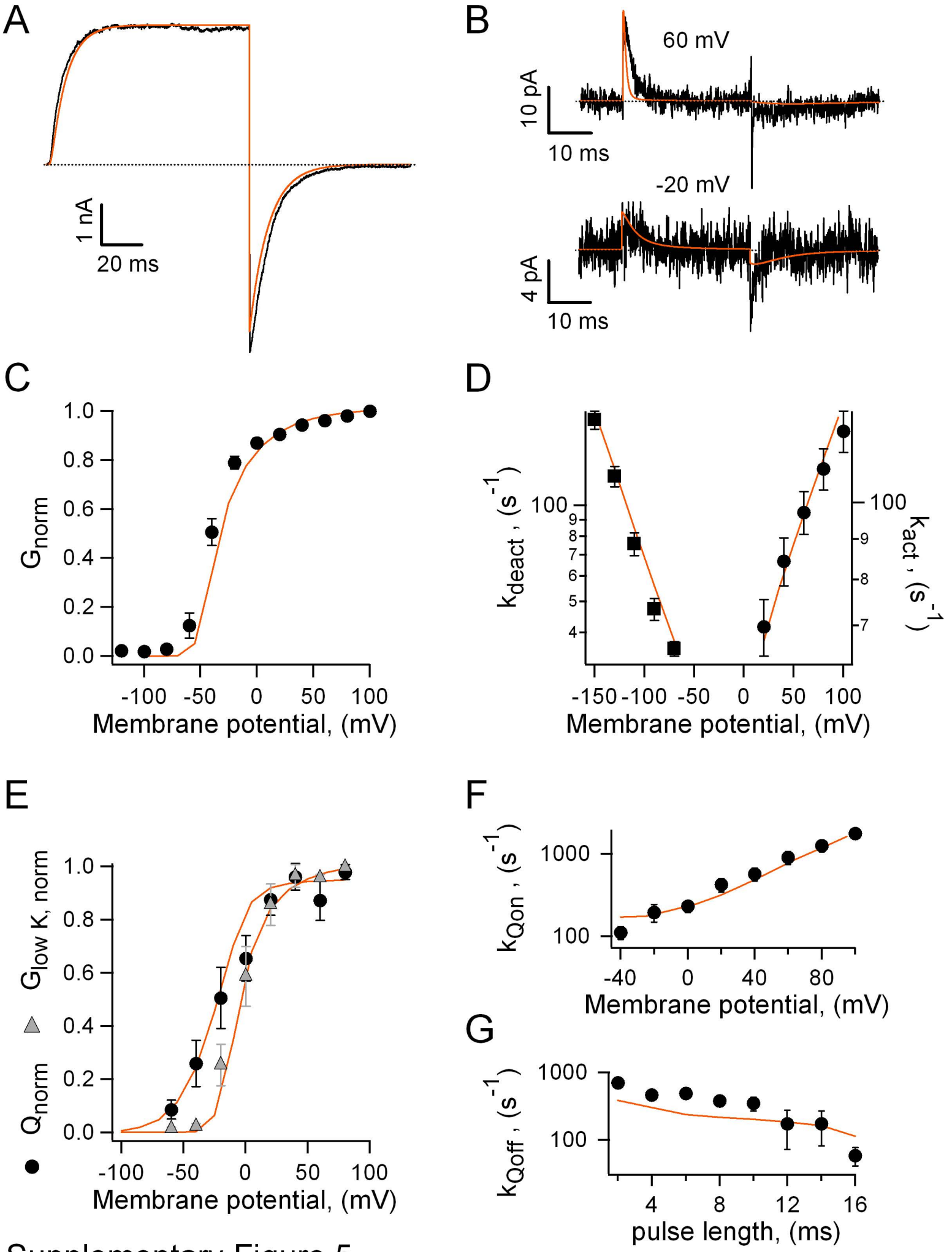

Supplementary Figure 5

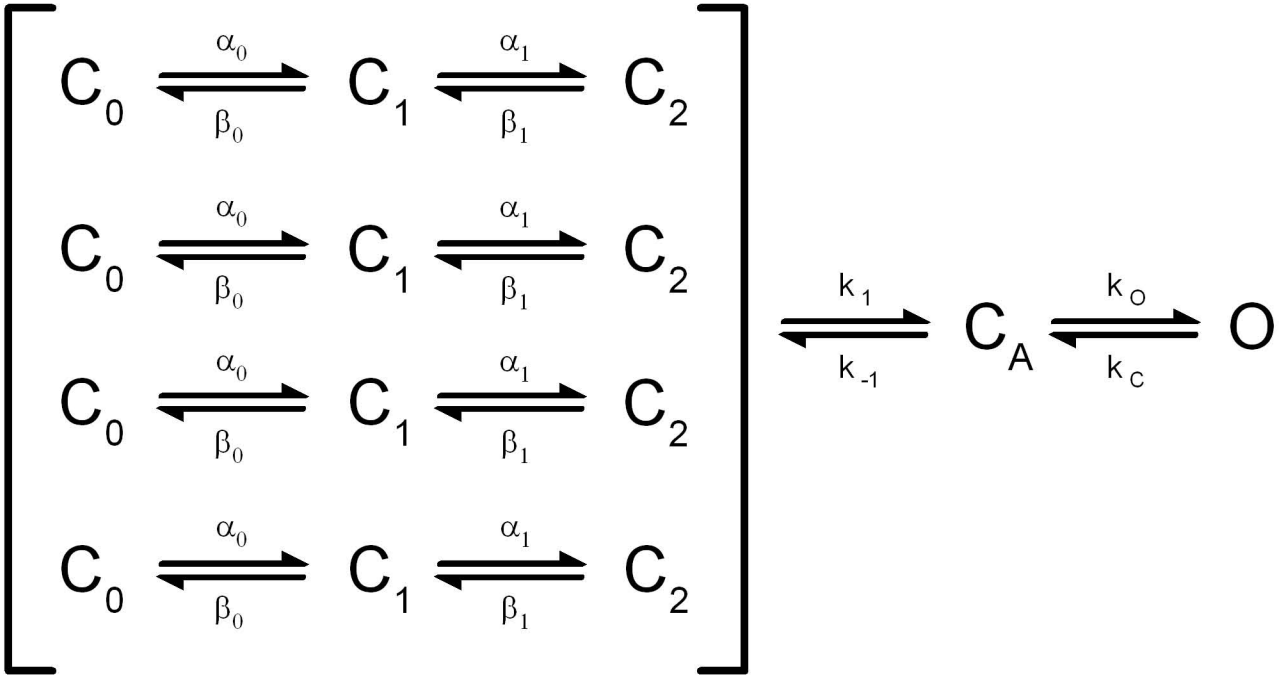

Supplementary Scheme I

SUPPLEMENTARY DATA

Supplementary Figure 1. CORM-2 inhibits the Kv2.1 channel in a CO-independent manner. (A) Time course of Slo1 activation at 80 mV by 0.12 mM CORM-2, obtained with 1 mM sodium dithionite alone (corm/dt) and with sodium dithionite and 0.1 mM deoxyhemoglobin (corm/Hb/dt). Sodium dithionite by itself (dt) or together with deoxyhemoglobin (Hb/dt) also activates the Slo1 channel. The presence of hemoglobin reduces the degree of activation of the channel by CORM-2 to that observed with sodium dithionite alone, confirming that hemoglobin can be adequately used as a CO-scavenger in our experiments. (B) Time course of inhibition of the Kv2.1 channel by 0.3 mM CORM-2 and 1mM sodium dithionite in the presence (corm/Hb/dt) or absence (corm/dt) of 0.25 mM deoxyhemoglobin at 100 mV. Hemoglobin does not make any difference in the CORM-2-mediated inhibition of the Kv2.1 channel, but the same degree of inhibition is observed when CORM-2 and sodium dithionite are applied together or when sodium dithionite is applied alone (dt), as if the sodium dithionite, but not hemoglobin, interfered with the effects of CORM-2. (C) Time course of inhibition of Kv2.1 currents by 1 mM sodium dithionite (1dt), 0.3 mM CORM-2 (corm), 1 mM sodium dithionite + 0.3 mM CORM-2 (corm/1dt) and 5 mM sodium dithionite (5dt). Pretreatment of the channel with sodium dithionite does not interfere with CORM-2-inhibition, indicating that the reducing agent does not covalently modify the channel to impede CORM-2 action. 5 mM sodium dithionite causes a larger reduction in current than 1 mM, which indicates that the inhibition of CORM-2 action by sodium dithionite is not due to a saturation of the effect by the reducing agent, which suggests that CORM-2 and sodium dithionite react and the resulting product is no longer able to inhibit the channel. Consistently, adding sodium dithionite to a concentrated CORM-2 solution causes effervescence and a rapid change of color from yellow to orange (data not shown). In any case, the presence or absence of CO, determined by the addition of hemoglobin, does not have an influence on Kv2.1 inhibition by CORM-2, suggesting that it is the donor molecule and not the CO it releases that has a modulatory effect on the channel. Dotted lines mark the zero-current level. Bovine blood methemoglobin (Sigma-Aldrich) solutions were prepared with recording solution and supplemented with 1 mM sodium dithionite (Sigma-Aldrich) to generate deoxyhemoglobin.

Supplementary Figure 2. eYFP-Kv2.1 mutant location and functional expression. (A) Amino acid sequence alignment between the rKv1.2 and rKv2.1Δ7 channels performed with the ClustalW2 Software. Yellow-shaded areas indicate transmembrane segment position. Black shading is for mutated residues located at the docking site between the VSD and the pore domain. Blue shading is for residues located at the docking site near the S6 PVP region. White characters indicate mutations with functional expression, while red characters mutants without functional expression. The numbering indicates the position of the mutated residues in the Kv1.2 (numbers below the sequence) and the Kv2.1 (numbers above) sequences. Letters directly above the Kv2.1 sequence indicate the amino acids by which the indicated residues were substituted. (B) Confocal microscopy fluorescence photos of WT and mutant eYFP-Kv2.1-expressing oocytes excited at 488 nm. Non-injected oocytes displayed no detectable fluorescence (data not shown).

Supplementary Figure 3. Properties of the G317V mutant in saline and CORM-2. (A) Representative variance vs mean current plot obtained from non-stationary noise analysis of G317V currents in saline at 100 mV. The red curve is a fit to the following equation: $\sigma^2 = iI\text{-}I^2/N$, where σ^2 is the current variance, I is the mean current, I is the single-channel current at 100 mV and N is the number of channels in the patch. The open probability P_o was calculated from: $P_o=I/(Ni)$, where I is the mean steady-state current at 100 mV. The obtained parameters are: i = 1.11 ± 0.10 pA and P_o = 0.12 ± 0.02 (n = 3). (B) Representative time course of CORM-2-effects on the G317V mutant at 100 mV measured from a train of 200 ms pulses from a holding potential

of -90 mV. CORM-2 applications are indicated by the black thick bars. The dotted line indicates de zero-current level and the arrows indicate the time points at which the current in (C) were measured. (C) Currents activated by voltage-pulses taken from the pulse-sequence shown in (B) in the absence and presence of CORM-2. (D) G317V currents activated by voltage ramps from -100 to 60 mV with 0.48 mV/s in the absence (black trace) and presence (grey trace) of 0.7 mM CORM-2. The red line is a fit to a single-barrier permeation model to the data between 30 and 60 mV. The model is described by the following equation: $I(V)=G_a K_i e^{-(1-\delta)zV/(k_B T)} - K_o e^{\delta zV/(k_B T)}$, where $I(V)$ is the current as a function of voltage, G_a is an amplitude reflecting the height of the barrier in the absence of voltage, K_i and K_o are the intracellular and extracellular K^+ concentrations, respectively, δ is the electrical distance reflecting the position of the barrier, z is the charge of the permeating particle and was set to 1 e_0, V is the voltage and k_BT has its usual meaning. The employed parameters were: G_a = -6.9 nA/mM and δ = 0.273. The GV curve shown in Fig.8C is the quotient between the voltage-ramp current and the fit.

Supplementary Figure 4. Model predictions for ionic- and gating-currents in the absence and presence of CORM-2. (A) Representative Kv2.1-current traces activated at 100 mV and deactivated at -120 mV in saline (black trace) and in 0.7 mM CORM-2 (grey trace) and predictions from the model in Scheme I for saline (yellow trace) and CORM-2 (red trace). The parameters used are listed in Table I for high K^+-conditions. (B) Representative gating-current traces elicited at several voltages and repolarized to -90 mV in saline and in CORM-2, with the predictions of the model superimposed on the data. The parameters used are listed in Table I under low K^+-conditions. (C) Representative *Shaker* currents in saline and in 0.35 mM CORM-2 activated at 20 mV and deactivated at -120 mV. Model's predictions are superimposed on the data. (D) *Shaker*W434F gating current traces with superimposed model's predictions. Parameters for *Shaker* are also listed in Table I.

Supplementary Figure 5. 16-state model's predictions for Kv2.1 experimental observations in saline. (A) Representative Kv2.1-current traces activated at 100 mV and deactivated at -120 mV. (B) Representative gating-current traces elicited at 60 and 20 mV and repolarized to -90 mV. (C) Normalized conductance vs voltage-curve. (D) Kv2.1 activation and deactivation rate constants as a function of voltage from Fig.3 C. (E) Q_{on}-V curve and G-V curve at low K^+ from Fig.4C. (F) Gating current activation rates from Fig.4D. (G) Gating current-deactivation rates from Fig.4F. The predictions from the 16-state model in Supplementary Scheme I are depicted as orange curves. The employed parameters are listed in Supplementary Table I.

SUPPLEMENTARY TABLE 1

Parameter estimates for Supplementary Scheme I

	Kv2.1- saline	
	high K^+	low K^+
$\alpha_0(0)$	600	300
$\beta_0(0)$	300	
$\alpha_1(0)$	1400	800
$\beta_1(0)$	60	100
$k_1(0)$	280	
$k_{-1}(0)$	55	
$k_O(0)$	60	
$k_C(0)$	10	
$z\alpha_0(0)$	0.5	
$z\beta_0(0)$	-0.5	
$z\alpha_1(0)$	0.5	
$z\beta_1(0)$	-0.4	
$zk_1(0)$	0.3	
$zk_{-1}(0)$	-0.5	
$zk_O(0)$	0.2	
$zk_C(0)$	-0.5	